

Spatiotemporal dissipative solitons and vortices in a multi-transverse-mode fiber laser

Thawatchai Mayteevarunyoo¹, Boris A. Malomed^{2,3}, and Dmitry V. Skryabin^{3,4}

¹*Department of Electrical and Computer Engineering,
Faculty of Engineering, Naresuan University, Phitsanulok 65000, Thailand*

²*Department of Physical Electronics,
School of Electrical Engineering, Faculty of Engineering,
and Center for Light-Matter Interaction,
Tel Aviv University, Tel Aviv 69978, Israel*

³*ITMO University, St. Petersburg 197101, Russia and*

⁴*Department of Physics, University of Bath, Bath, BA2 7AY, UK*

Abstract

We introduce a model for spatiotemporal modelocking in multimode fiber lasers, which is based on the (3+1)-dimensional cubic-quintic complex Ginzburg-Landau equation (cGLE) with conservative and dissipative nonlinearities and a 2-dimensional transverse trapping potential. Systematic numerical analysis reveals a variety of stable nonlinear modes, including stable fundamental solitons and breathers, as well as solitary vortices with winding number $n = 1$, while vortices with $n = 2$ are unstable, splitting into persistently rotating bound states of two unitary vortices. A characteristic feature of the system is bistability between the fundamental and vortex spatiotemporal solitons.

I. INTRODUCTION AND THE MODEL

New physical principles for generating and controlling ultrashort pulses are under constant scrutiny of the scientific community. A recent prominent topic of the research in this area is complex multi-mode spatiotemporal dynamics in optical fibers used for both generation and delivery of short pulses, see, e.g., [1–4] for review. As intensity of light is increased through tighter focusing in both time and space, it starts interacting with matter nonlinearly, which is crucially important for the generation of ultrashort pulses and their spectral and temporal shaping. While the structure of the short pulses is intrinsically multimode (in a cavity) and multi-wavelength in the propagation direction (in free space), their transverse multimode structure has been traditionally considered as a thing to avoid and a special care is commonly taken to ensure that a pulse is carried by a single transverse mode. Nevertheless, transversely multimode ultrashort pulses have recently become a topic of intense research. Their spatial complexity is a feature to be controlled and utilized [2], fiber-based devices being the most prominent setting in this context. In particular, multi-transverse-mode passive fibers have been used for boosting transmission capacity of communication lines by means of spatial-division multiplexing [5]. Strongly nonlinear propagation of pulses in graded-index (GRIN) fibers with a transversely parabolic refractive index has been investigated in the context of the beam-profile self-cleaning, as well as the generation of continuum radiation and solitons [6–14]. Spatiotemporal mode-locking (STML) of longitudinal and transverse modes in a fiber-laser system was recently reported in [41], with follow-up results contributing to this area. Those include observations of solitons and soliton bound states [15, 16], a proposal for the multi-transverse-mode gain-saturation mechanism [17], and direct generation of vortex beams [18]. The latter result is directly relevant and motivational for the present work, though the above-mentioned recent STML results predominantly dealt with the normal-GVD (group-velocity-dispersion) case, while we address the case of anomalous GVD in this work. Previously, this case has been chiefly considered in studies with suppressed transverse effects [1]. Multimode fibers are closely related to multi-core ones, since coupled cores introduce multiple transverse modes, whose number is equal the numbers of cores. Pulse compression, light bullets and spatiotemporal discrete vortices all have been studied in the multi-core fibers [19–21]. STML in various multi-core waveguide systems has also been addressed by several groups [22–24]. It is relevant to mention that studies of STML

and soliton effects in (non-fiber) laser cavities had started decades ago—see, e.g., [25–27].

Mode-locking effects and formation of dissipative solitons have been traditionally (and successfully) modeled using various realizations of the complex Ginzburg-Landau equation (cGLE), its ubiquitous version being one with the cubic-quintic nonlinearity [1, 28]. The quintic term supports the subcritical transition to the lasing state, thereby providing conditions for mode-locking and the creation of stable solitons at subcritical pumping levels [28]. Locking of the longitudinal modes in single-transverse-mode fiber lasers is described by (1+1)-dimensional cGLE, while the consideration of multi-mode fibers opens the way to the realm of the (3+1)D cGLE. The lateral confinement of the fiber modes immediately requires inclusion of the trapping potential acting in two transverse dimensions, which is a basic parabolic potential for GRIN fibers. This potential is a feature creating a new playground relative to the quite extensive studies of “light bullets” [29–32] and vortex solitons [33–37] in (3+1)D cGLE. Below we use the (3+1)D cGLE including conservative and dissipative cubic-quintic terms and a 2D parabolic potential.

Measuring the propagation distance along the fiber, beam’s width, and time in units of suitably defined scales L , w and τ , the cGLE is written as

$$i\frac{\partial\psi}{\partial z} + \frac{L}{2\tau^2}k''(1-i\beta)\frac{\partial^2\psi}{\partial t^2} + \frac{L}{2k_0w^2}\left(\frac{\partial^2}{\partial x^2} + \frac{\partial^2}{\partial y^2}\right)\psi - \frac{k_0gw^2L}{2}(x^2+y^2)\psi + iL\varepsilon'\psi + L(\eta' - i\alpha')|\psi|^2\psi + L(\nu' + i\mu')|\psi|^4\psi = 0. \quad (1)$$

Here z , t and x, y are the dimensionless distance, time, and transverse coordinate, and time is defined in the reference frame moving with the pulse’s group velocity. Further, k'' is the GVD coefficient, β the spectral-filtering coefficient, k_0 the propagation constant of the fundamental mode, g the GRIN parameter, and $\varepsilon \equiv L\varepsilon' > 0$ the dimensionless linear loss over length L . If ψ is the dimensionless field envelope, then the scaled (dimensionless) parameters $\eta = L\eta'$, $\alpha = L\alpha' > 0$, $\nu = L\nu'$ and $\mu = L\mu' > 0$ determine ratios between L and the nonlinear lengths associated with the Kerr effect, cubic gain, quintic nonlinearity, and nonlinear saturation, respectively. We now fix $L = 1/(k_0gw^2)$, $w^2 = L/k_0$ and $\tau^2 = Lk''$ to write the spatiotemporal cGLE (1) with the cubic-quintic terms in the scaled form:

$$i\frac{\partial\psi}{\partial z} + \frac{1}{2}(1-i\beta)\frac{\partial^2\psi}{\partial t^2} + \frac{1}{2}\left(\frac{\partial^2}{\partial x^2} + \frac{\partial^2}{\partial y^2}\right)\psi - (x^2+y^2-i\varepsilon)\psi + (\eta-i\alpha)|\psi|^2\psi + (\nu+i\mu)|\psi|^4\psi = 0. \quad (2)$$

Nontrivial solutions can be supported by the cubic gain in the competition with the linear

and quintic losses, if the gain coefficient exceeds a threshold value [39]

$$\alpha = A\alpha_{\text{thr}}, \quad \alpha_{\text{thr}} \equiv (2\sqrt{\varepsilon\mu}) \quad (3)$$

with $A > 1$. We here fix values $A = 1.5$ and $\beta = \nu = 0$, which adequately represent the generic case, while the linear loss and nonlinear gain, ε and μ , are varied.

Thus, in this work we focus on predicting STML scenarios in the setup based on the interplay of the cubic-quintic dissipative nonlinearity with the anomalous GVD, transverse diffraction, parabolic GRIN potential, and Kerr self-focusing, in the absence of temporal and spatial filtering. In fact, the prediction of patterns which are stable without the help of the filtering is an essential novelty of the analysis.

II. NUMERICAL RESULTS

We look for stationary localized solutions, in the form of $\psi(x, y, t, z) = \phi(x, y, t) \exp(iqz)$, where q is a real propagation constant, and function $\phi(x, y, t)$ satisfies the equation following from the substitution of this ansatz in Eq. (2) with $\beta = \nu = 0$:

$$-q\phi + \frac{1}{2} \left(\frac{\partial^2}{\partial t^2} + \frac{\partial^2}{\partial x^2} + \frac{\partial^2}{\partial y^2} \right) \phi - (x^2 + y^2 - i\varepsilon) \phi + (\eta - i\alpha) |\phi|^2 \phi + i\mu |\phi|^4 \phi = 0. \quad (4)$$

Splitting complex equation (4) into real and imaginary parts, solutions for localized states have been produced by means of the modified squared-operator method [40]. The solutions are characterized by the value of their total energy, i.e., integral norm,

$$P = \int \int \int |\psi(x, y, t)|^2 dx dy dt. \quad (5)$$

A. Fundamental dissipative solitons

To determine numerical solutions and the propagation constant simultaneously, the Gaussian input was used, $\phi_0 = 1.5 \operatorname{sech}(x^2 + y^2) \exp(-1/2t^2)$. The existence and stability of numerically found fundamental (zero-vorticity) dissipative solitons, produced by Eq. (4), is summarized in Fig. 1(a), which displays the numerically found q and P (integral power) vs. the linear-loss parameter, ε , for a fixed value of the quintic-loss coefficient, $\mu = 1$, while the cubic gain is fixed as per Eq. (3). The stability was identified by means of systematic simulations of perturbed evolution of the solitons in the framework of Eq. (2). Figure 1(b)

summarizes the results by plotting stability boundaries for the dissipative solitons in the plane of (μ, ε) . The shape and evolution of the stable solitons are illustrated by Fig. 2.

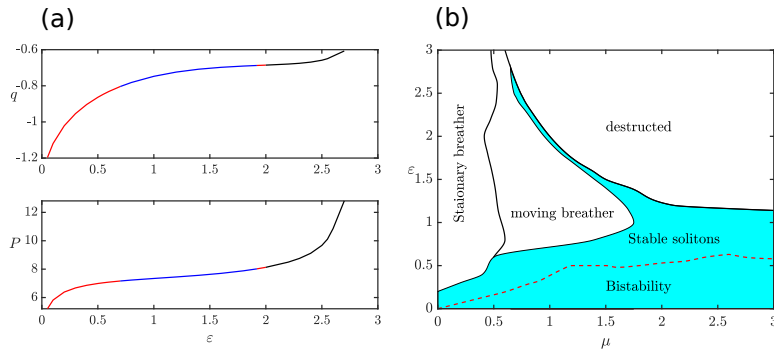


FIG. 1: (a) Numerically computed propagation constant q and integral power P [see Eq. (5)] of fundamental three-dimensional solitons versus ε , for fixed $\mu = 1$ in Eq. (2). Red, blue and black segments correspond to stable fundamental solitons, moving breathers, and eventually destroyed modes, respectively. (b) The stability chart for the stationary fundamental solitons and modes into which unstable solitons are spontaneously transformed. Indicated inside the stability area of solitons is the bistability region, in which solitary vortices with winding numbers are stable too, cf. Fig. 5(b).

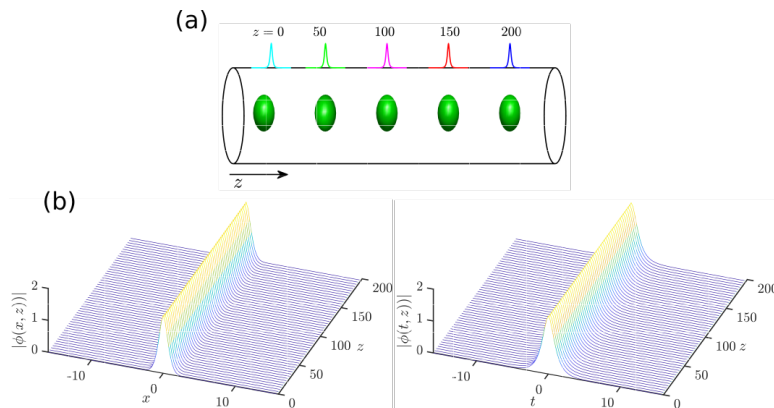


FIG. 2: (a) The evolution of a stable fundamental soliton, for $\mu = 1, \varepsilon = 0.5$, with $q = -0.8635, P = 6.9898$, is displayed by means of isosurfaces of $|\psi(x, y, z, t)|$. (b) Left and right panels display spatial and temporal cross sections of the soliton's shape, $|\psi(x, 0, z, 0)|$ and $|\psi(0, 0, z, t)|$, respectively.

Weakly unstable fundamental solitons can be easily found too. They spontaneously transform into quiescent or moving breathers, see examples in Fig. 3 and 4, respectively. The breathers are robust dynamical modes, which keep integrity in the course of indefinitely

long subsequent evolution. Their stability regions in the parameter plane of (μ, ε) are also drawn in Fig. 1(b). Note, in particular, that the region of destruction of all modes (i.e., onset of spatial “turbulence” as a result of the simulated evolution) occupies, quite naturally, an area in which the loss and gain coefficients [recall that the latter one is taken as per Eq. (3)] are too large to maintain the stability of regular modes, such as solitons and breathers. The same peculiarity is observed in stability charts displayed below for vortex states in Figs. 5(b) and 10(b).

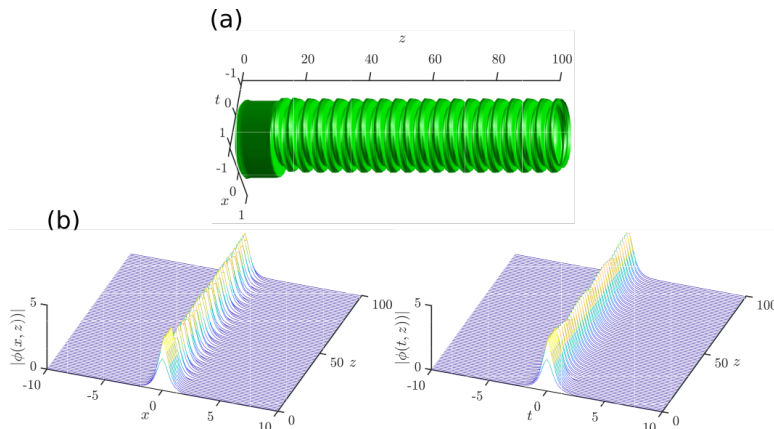


FIG. 3: (a) The evolution of a robust quiescent breather, into which an unstable fundamental soliton transforms for $\mu = 0.3, \varepsilon = 2.8$, which corresponding to $q = -2.0446, P = 5.3081$, shown by means of the isosurface of $|\psi(x, y, z, t)|$. (b) Left and right panels show the evolution in the spatial and temporal of cross sections, $|\psi(x, 0, z, 0)|$ and $|\psi(0, 0, z, t)|$, respectively.

B. Vortices with winding number $n = 1$

Localized vortex states with winding number (topological charge) $n = 1$ were constructed as solutions of Eq. (4), starting with input, written in polar coordinates (r, θ) (in the plane of (x, y)) as $\phi_0 = 2.5r \operatorname{sech}(r^2) \operatorname{sech}(t) \exp(i\theta)$. As a result, two coexisting vortex families, one unstable and one stable, have been found. Figure 5(a) displays the respective numerically found values of q and integral power P versus ε . In particular, the stable (red) branch was found in the interval of $0 < \varepsilon < 0.4$ for $\mu = 1.0$. Unstable vortex states split into fundamental solitons (in the blue segment), or transform into chaotically oscillating modes (magenta) or moving breathers, which keep the initial vorticity (yellow), or suffer destruction (black). The results are summarized in Fig. 5(b) in terms of the (μ, ε) plane, where the shaded area

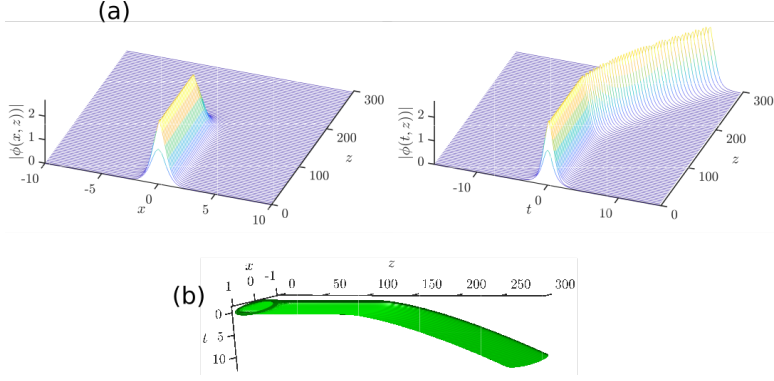


FIG. 4: A robust moving breather for $\mu = 1.0, \varepsilon = 1.8$, into which the respective unstable soliton, with $q = -1.7927, P = 4.5920$, spontaneously transforms. (a) The evolution in the spatial and temporal cross sections, $|\psi(x, 0, z, 0)|$ (left) and $|\psi(0, 0, z, t)|$ (right). (b) The spatiotemporal dynamics with temporal motion.

pertains to chaotically oscillating modes. Typical examples of the stable vortices, splitting, chaotically oscillating modes, and moving vortex breathers are shown in Fig. 6, 7, 8 and 9, respectively.

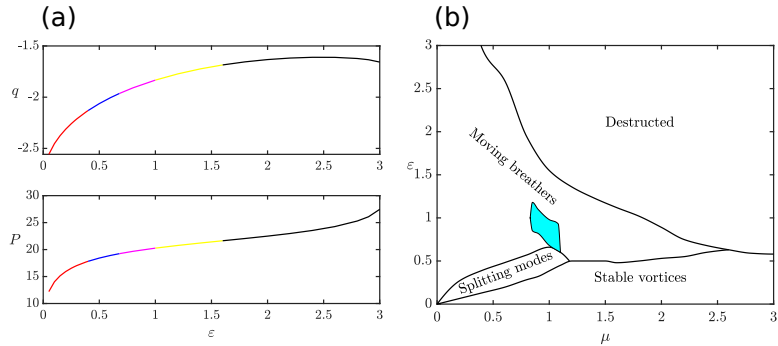


FIG. 5: (a) The numerically found values of q (top panel) and P (bottom panel) for stationary vortices with winding number $n = 1$ versus ε for fixed $\mu = 1.0$. Red, blue, magenta, yellow and black segments correspond to stable vortices, splitting into fundamental solitons, chaotically oscillating modes, moving vortex breathers, and destruction of unstable vortices, respectively. (b) The stability chart for vortices with $n = 1$ in the plane of (μ, ε) . The central shaded area in (b) is populated by chaotically oscillating localized modes, see an example in Fig. 8. Note that the stability area of vortices is completely covered by the region in which the fundamental solitons are stable [cf. Fig. 1(b)], i.e., it is a bistability area.

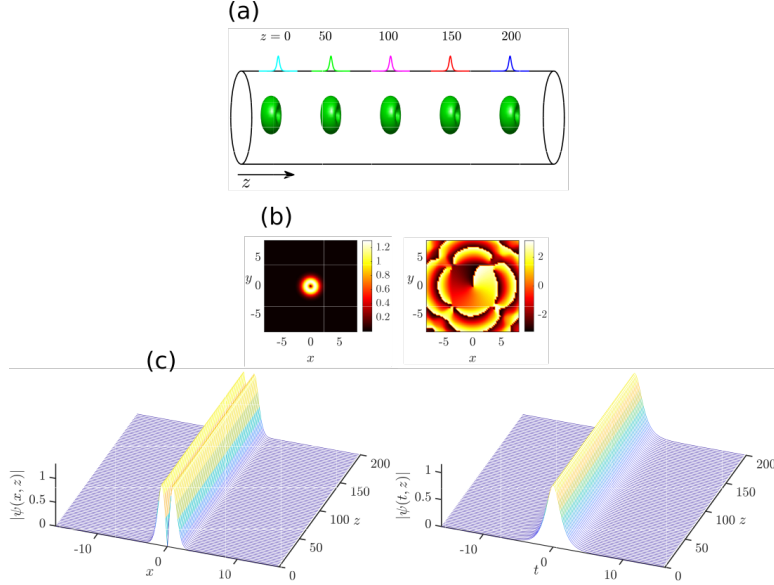


FIG. 6: (a) The isosurface evolution of a stable vortex found at $\mu = 1.0, \varepsilon = 0.2$, which corresponds to $q = -2.3130, P = 15.9142$. (b) Its amplitude and phase patterns (c) Left and right panels display the evolution of the spatial and temporal cross sections $|\psi(x, 0, z, 0)|$ and $|\psi(0, 0, z, t)|$, respectively.

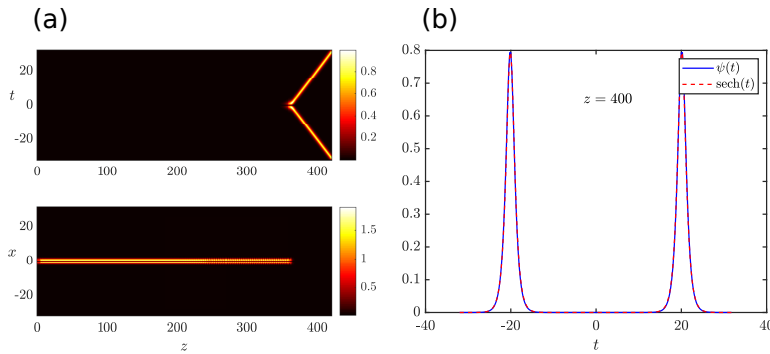


FIG. 7: The spontaneous splitting of an unstable vortex with $n = 1$ into two fundamental solitons, at $\mu = 1.0, \varepsilon = 0.6$. (a) The evolution of $|\psi|$ is shown in the t - and x -cross sections (top and bottom panels, respectively). (b) The temporal shape of the moving fundamental solitons, produced by the splitting, at $z = 400$ (the blue line), fitted to the standard soliton's shape, $\text{sech}(t)$.

An obviously important conclusion, demonstrated by the comparison of Figs. 5(b) and 1(b), is the bistability between the fundamental solitons and solitary vortices, as the solitons' stability area completely covers that of the vortices. In fact, this feature may be interpreted as tri-stability, as stable vortices may have winding numbers $+1$ and -1 . This fact may find

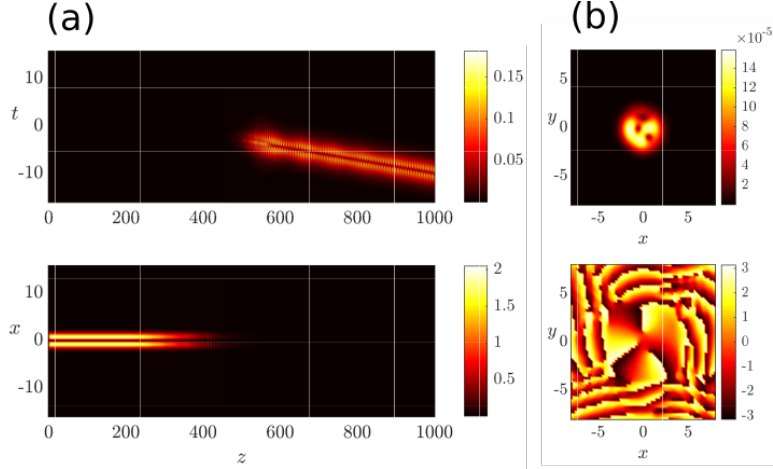


FIG. 8: (a) The evolution of $|\psi(0,0,z,t)|$ and $|\psi(x,0,z,0)|$ in the t - and x - cross-sections, illustrating the spontaneous transformation of an unstable stationary vortex with $n = 1$ into a chaotically oscillating mode at $\mu = 1.0, \varepsilon = 0.9$. (b) The respective amplitude and phase patterns at $z = 1000$ (eventual values of the amplitude are small, as a result of the evolution).

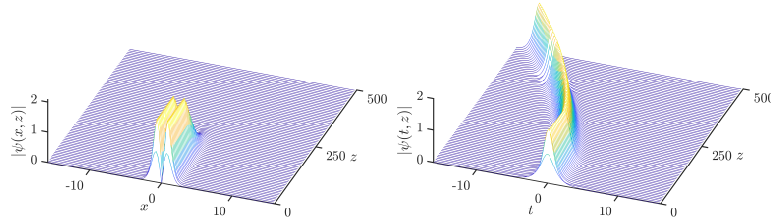


FIG. 9: A moving breather, into which an unstable stationary vortex, with $q = -2.9276, P = 9.9546$, is spontaneously transformed (keeping its vorticity) at $\mu = 1.0, \varepsilon = 1.2$. The evolution of cross sections $|\psi(x,0,z,0)|$ and $|\psi(0,0,z,t)|$ is displayed in the left and right panels, respectively.

applications to optical switching in the multimode fibers, and is of considerable interest in terms of general properties of vortex solitons in dissipative media. The switching may be controlled by adjusting the power: it is seen in the bottom panels of Figs. 1(a) and 5(a) that the power of a stable vortex is $\simeq 3$ times larger than the power of a coexisting stable fundamental soliton.

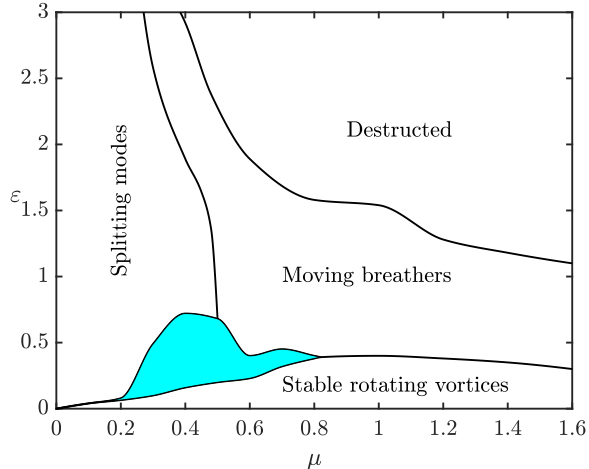


FIG. 10: The stability chart in the plane of (μ, ε) for vortices with $n = 2$. The shaded area corresponds to the “wobbling breathers”.

C. Vortices with $n = 2$

Double vortices, with winding number $n = 2$, were constructed as solutions of Eq. (4), starting with input $\phi_0 = 2.5r \operatorname{sech}(r^2) \operatorname{sech}(t) \exp(2i\theta)$. Systematic simulations have demonstrated that no double vortices are stable. They spontaneously develop into various modes, which are robust in different areas in the plane of (μ, ε) , as shown in Fig. 10. These are rotating bound states of two unitary vortices, into which the double vortex splits, which is shown in Fig. 11; “wobbling breathers”, which lose the original vorticity and perform spontaneous shuttle motion in the x direction, coupled to intrinsic vibrations, see Fig. 12; and moving breathers (not shown here in detail), which lose the initial vorticity. In addition, there is a parameter region in which the double vortex splits into 2, 3, or 4 breathers (each without intrinsic vorticity), see details in Fig. 13.

III. CONCLUSIONS

In this work, we have proposed and investigated a model for the passively mode-locked laser, based on the graded-index nonlinear multimode fiber. The model is based on the $(3+1)$ D cGLE (complex Ginzburg-Landau equation) with the complex cubic-quintic nonlinearity and the transverse two-dimensional trapping potential, which represents the graded-index structure. A novelty in comparison with previously studied models is that stable stationary

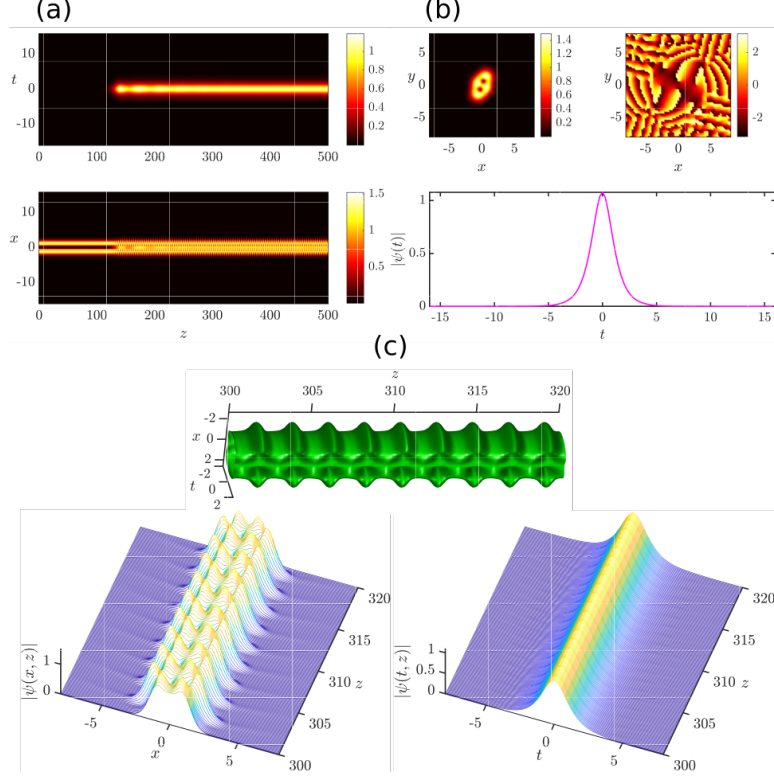


FIG. 11: Spontaneous splitting of an unstable vortex with $n = 2$ into a stably rotating bound state of two vortices with $n = 1$ at $\mu = 0.4$, $\varepsilon = 0.1$ (a) The evolution of the field in the temporal and spatial cross sections, $|\psi(0, 0, z, t)|$ and $|\psi(x, 0, z, 0)|$. (b) Amplitude and phase patterns of $\psi(x, y)$ in the plane of $t = 0$ and (bottom) the temporal profile at the central point, $x = y = 0$, plotted at $z = 500$ (c) The top, left and right panels zoom in on the evolution of the absolute value of the field, and spatial and temporal cross sections, respectively, in the interval of $300 < z < 320$. The established evolution (rotation) period is $T_z = 2.2$.

and dynamical modes are found in the absence of the spatial and temporal filtering in the model.

The systematic numerical analysis reveals a variety of lasing regimes, including fundamental $(3 + 1)$ D solitons and breathers, as well as stable solitary vortices with winding number $n = 1$, that can also exhibit a splitting instability leading to formation of two fundamental solitons. The vortices with $n = 2$ are found to be unstable against splitting into a rotating bound state of two unitary vortices. A remarkable feature of the system is the coexistence of between the stable fundamental solitons and vortices with $n = 1$. A variety of operation regimes reported here, and a possibility of their implementation in practical

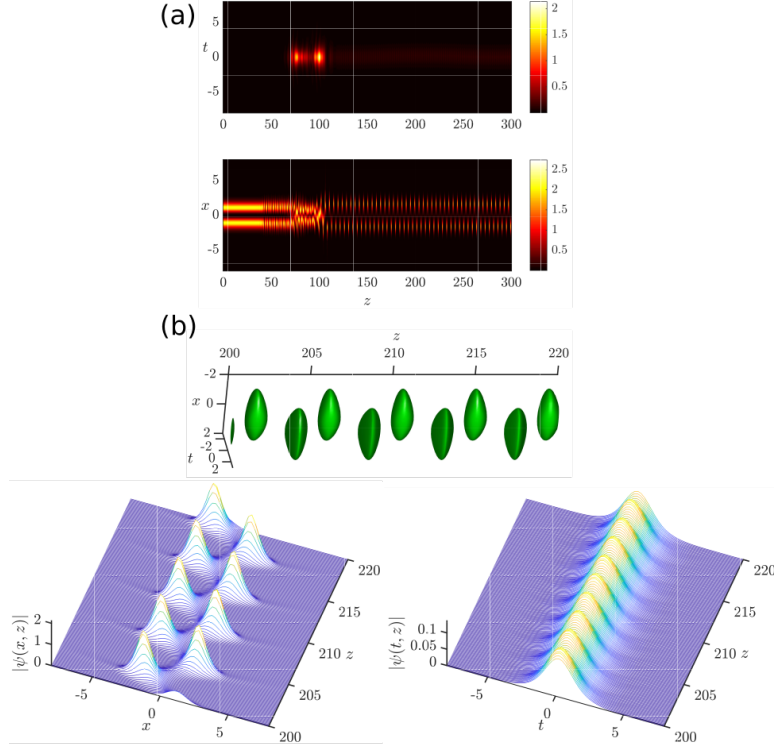


FIG. 12: The “wobbling breather” at $\mu = 0.4$, $\varepsilon = 0.6$ (a) The evolution of the field in the temporal and spatial cross sections, $|\psi(0, 0, z, t)|$ and $|\psi(x, 0, z, 0)|$. (b) The top, left and right panels zoom in on the evolution of the absolute value of the field, and spatial and temporal cross sections in the interval of $z = 200 - 220$, respectively. The established evolution period is $T_z = 4.5$.

devices is expected to assist the development of methods to optimize and tune temporal, spatial and spectral characteristics of short spatiotemporal pulses generated in multimode fiber lasers.

Funding

Thailand Research Fund (grant BRG6080017); Russian Foundation for Basic Research (17-02-00081); Israel Science Foundation (grant 1287/17).

[1] P. Grelu, N. Akhmediev, “Dissipative solitons for mode-locked lasers,” *Nature Photonics* **6**(2), 84–92 (2012)

- [2] W. Fu, L. G. Wright, P. Sidorenko, S. Backus, and F. W. Wise, “Several new directions for ultrafast fiber lasers [Invited],” *Opt. Express* **26**(8), 9432-9463 (2018)
- [3] L. G. Wright, Z. M. Ziegler, P. M. Lushnikov, and Z. Zhu, “Multimode Nonlinear Fiber Optics: Massively Parallel Numerical Solver, Tutorial, and Outlook,” *IEEE J. Sel. Top. Quantum Electron.*, **24**(3), 5100516 (2018)
- [4] C. Jauregui, J. Limpert, and A. Tünnermann, “High-power fibre lasers,” *Nature. Photonics* **7**(11), 861–867 (2013).
- [5] D. Richardson, J. Fini, and L. Nelson, “Space-division multiplexing in optical fibres,” *Nature. Photonics* **7**(5), 354–362 (2013).
- [6] Z. Liu, L. G. Wright, D. N. Christodoulides, and F. W. Wise, “Kerr self-cleaning of femtosecond-pulsed beams in graded-index multimode fiber,” *Opt. Lett.* **41**(16), 3675–3678 (2016).
- [7] K. Krupa, A. Tonello, B. M. Shalaby, M. Fabert, A. Barthélémy, G. Millot, S. Wabnitz, and V. Couderc, “Spatial beam self-cleaning in multimode fibres,” *Nature. Photonics* **11**(4), 237–241 (2017).
- [8] A. S. Ahsan, and G. P. Agrawal. “Graded-index solitons in multimode fibers,” *Opt. Lett.* **43**, 3345-3348 (2018).
- [9] L. G. Wright, W. H. Renninger, D. N. Christodoulides, and F. W. Wise, “Spatiotemporal dynamics of multimode optical solitons,” *Opt. Express* **23**, 3492-3506 (2015).
- [10] O. V. Shtyrina, M. P. Fedoruk, Y. S. Kivshar, and S. K. Turitsyn, “Coexistence of collapse and stable spatiotemporal solitons in multimode fibers,” *Phys. Rev. A* **97**, 013841 (2018).
- [11] L. G. Wright, D. N. Christodoulides, and F. W. Wise, “Controllable spatiotemporal nonlinear effects in multimode fibres,” *Nature. Photonics* **9**(5), 306–310 (2015).
- [12] Z. Zhu, L. G. Wright, D. N. Christodoulides, and F. W. Wise, “Observation of multimode solitons in few-mode fiber,” *Opt. Lett.* **41**(20), 4819–4822 (2016).
- [13] W. H. Renninger and F. W. Wise, “Optical solitons in graded-index multimode fibres,” *Nature. Commun.* **4**, 1719 (2013).
- [14] K. Krupa, A. Tonello, A. Barthélémy, V. Couderc, B. M. Shalaby, A. Bendahmane, G. Millot, and S. Wabnitz, “Observation of geometric parametric instability induced by the periodic spatial self-imaging of multimode waves,” *Phys. Rev. Lett.* **116**(18), 183901 (2016).
- [15] H. Qin, X. Xiao, P. Wang, and C. Yang, “Observation of soliton molecules in a spatiotemporal

- mode-locked multimode fiber laser,” *Opt. Lett.* **43**(9), 1982-1985 (2018)
- [16] Y. Ding, X. Xiao, P. Wang, and C. Yang, “Multiple-soliton in spatiotemporal mode-locked multimode fiber lasers,” *Opt. Express* **27**(8), 11435-11446 (2019)
- [17] T. Chen, Q. Zhang, Y. Zhang, and X. Li, “All-fiber passively mode-locked laser using nonlinear multimode interference of step-index multimode fiber,” *Photon. Res.* **6**, 1033-1039 (2018)
- [18] D. Mao, M. Li, Z. He, X. Cui, H. Lu, W. Zhang, H. Zhang, and J. Zhao, “Optical vortex fiber laser based on modulation of transverse modes in two mode fiber,” *APL Photonics* **4**(6), 060801 (2019)
- [19] I. S. Chekhovskoy, A. M. Rubenchik, O. V. Shtyrina, and M. P. Fedoruk, “Nonlinear combining and compression in multicore fibers,” *Phys. Rev. A* **94**(4), 043848 (2016)
- [20] S. Minardi, F. Eilenberger, Y. V. Kartashov, “Three-Dimensional Light Bullets in Arrays of Waveguides,” *Phys. Rev. Lett.* **105**(26), 263901 (2010)
- [21] F. Eilenberger, K. Prater, S. Minardi, R. Geiss, U. Röpke, J. Kobelke, K. Schuster, H. Bartelt, S. Nolte, A. Tünnermann, and T. Pertsch, “Observation of discrete, vortex light bullets”, *Phys. Rev. X* **3**, 041031 (2013)
- [22] H. G. Winful and D. T. Walton, “Passive mode locking through nonlinear coupling in a dual-core fiber laser,” *Opt. Lett.* **17**(23), 1688–1690 (1992).
- [23] J. Proctor and J. N. Kutz, “Nonlinear mode-coupling for passive mode-locking: application of waveguide arrays, dual-core fibers, and/or fiber arrays,” *Opt. Express* **13**(22), 8933–8950 (2005).
- [24] T. F. S. Büttner, D. D. Hudson, E. C. Mägi, A. C. Bedoya, T. Taunay, and B. J. Eggleton, “Multicore, tapered optical fiber for nonlinear pulse reshaping and saturable absorption,” *Opt. Lett.* **37**(13), 2469–2471 (2012).
- [25] D. Auston, “Transverse mode locking,” *IEEE J. Quant. Electron* **4**, 420-422 (1968).
- [26] P. W. Smith, “Simultaneous phase-locking of longitudinal and transverse laser modes,” *Appl. Phys. Lett.* **13**, 235 (1968).
- [27] A. M. Dunlop, W. J. Firth, E. M. Wright, “Master equation for spatiotemporal beam propagation and Kerr lens mode-locking,” *Opt. Commun.* **138**, 211-226 (1997)
- [28] N. Akhmediev and A. Ankiewicz, eds., *Dissipative solitons*, Vol. 661 of Lecture Notes in Physics (Springer, 2005).
- [29] S. Raghavan, and G. P. Agrawal, “Spatiotemporal solitons in inhomogeneous nonlinear me-

- dia,” *Opt. Commun.* **180**, 377-382 (2000).
- [30] N. Akhmediev, J. M. Soto-Crespo, P. Grelu, “Spatiotemporal optical solitons in nonlinear dissipative media: From stationary light bullets to pulsating complexes,” *Chaos* **17** 037112 (2007)
- [31] N. B. Aleksić, V. Skarka, D. V. Timotijević, and D. Gauthier, “Self-stabilized spatiotemporal dynamics of dissipative light bullets generated from inputs without spherical symmetry in three-dimensional Ginzburg-Landau systems,” *Phys. Rev. A* **75**, 061802 (2007)
- [32] S. Chen, “Analytical spinless light-bullet solutions as attractive fixed points in the three-dimensional cubic-quintic complex Ginzburg-Landau equation,” *Phys. Rev. A* **86**, 033829 (2012)
- [33] D. Mihalache, D. Mazilu, F. Lederer, H. Leblond, “Stability limits for three-dimensional vortex solitons in the Ginzburg-Landau equation with the cubic-quintic nonlinearity,” *Phys. Rev. A* **76**, 045803 (2007)
- [34] D. Mihalache, D. Mazilu, F. Lederer, H. Leblond “Collisions between coaxial vortex solitons in the three-dimensional cubic-quintic complex Ginzburg-Landau equation,” *Phys. Rev. A* **77**(3) (2008)
- [35] B. Liu, Y.-F. Liu, X.-D. He, “Impact of phase on collision between vortex solitons in three-dimensional cubic-quintic complex Ginzburg-Landau equation,” *Opt. Express* **22**, 26203-26211 (2014)
- [36] N. A. Veretenov, S. V. Fedorov, N. N. Rosanov, “Topological Vortex and Knotted Dissipative Optical 3D Solitons Generated by 2D Vortex Solitons,” *Phys. Rev. Lett.* **119**(26), 263901 (2017)
- [37] B. A. Malomed, “(INVITED)Vortex solitons: Old results and new perspectives”, *Physica D* **399**, 108-137 (2019)
- [38] T. Mayteevarunyoo, B. A. Malomed, and D. V. Skryabin, “One- and two-dimensional modes in the complex Ginzburg-Landau equation with a trapping potential,” *Opt. Express* **26**, 8849-8865 (2018).
- [39] T. Mayteevarunyoo, B.A. Malomed and D. Skryabin, “Vortex modes supported by spin-orbit coupling in a laser with saturable absorption,” *New J. Phys.* **20**, 113019, 2018.
- [40] J. Yang, *Nonlinear Waves in Integrable and Nonintegrable Systems* (SIAM: Philadelphia, 2010).

- [41] L. G. Wright, D. N. Christodoulides, and F. W. Wise, “Spatiotemporal mode-locking in multimode fiber lasers,” *Science* **358**(6359), 94-97 (2017).

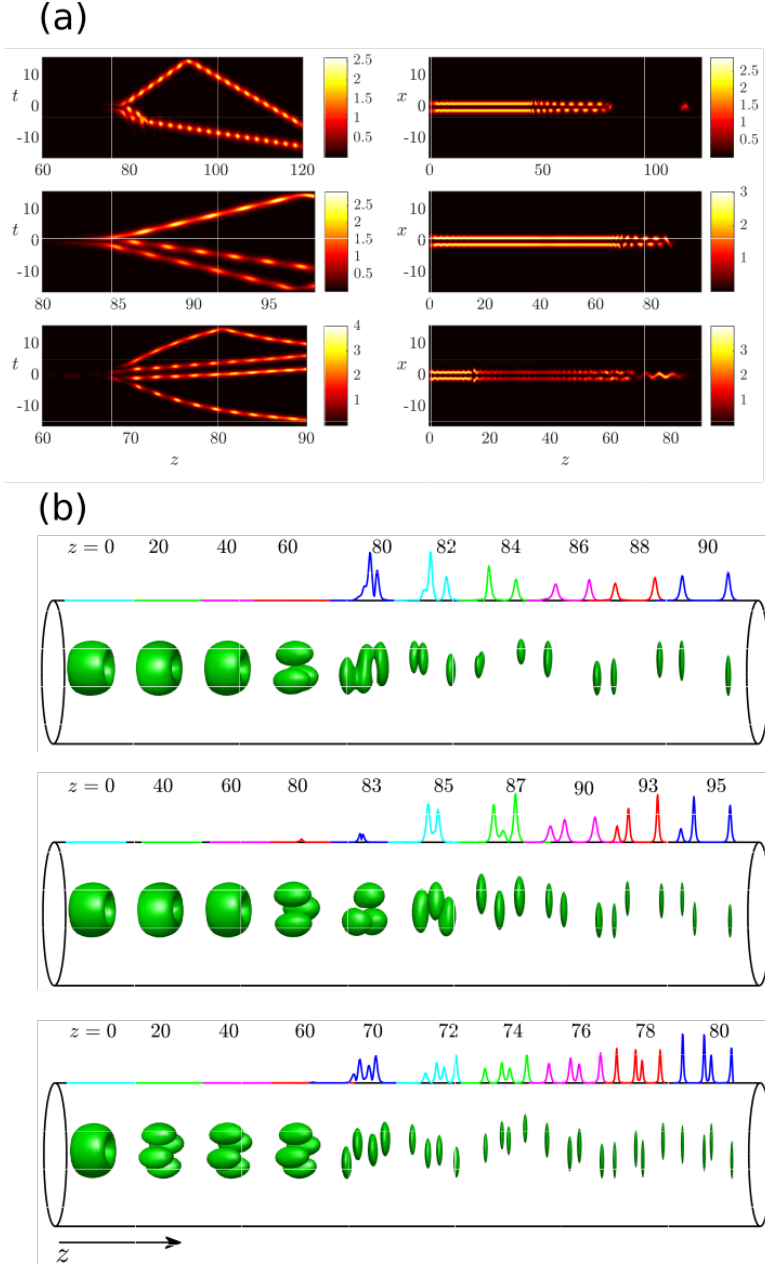


FIG. 13: (a) Splitting of an unstable breather with $n = 2$ into 2, 3 and 4 secondary breathers with zero intrinsic vorticity at $\mu = 0.4, \varepsilon = 0.9$ (top), $\mu = 0.4, \varepsilon = 1.4$ (middle), and $\mu = 0.2, \varepsilon = 3.0$ (bottom), displayed by means of temporal cross sections, $|\psi(0, 0, z, t)|$. Panels in the right column display the respective evolution in the spatial cross section, $|\psi(x, 0, z, 0)|$. (b) The same as (a) but illustrating the isosurface evolution in 3D.